^{1}H and ^{13}C NMR of Multilamellar Dispersions of Polyunsaturated (22:6) Phospholipids

Sarah Everts and James H. Davis
Department of Physics, University of Guelph, Guelph, Ontario N1G 2W1, Canada

ABSTRACT   The polyunsaturated fatty acid docosahexaenoic acid (DHA) makes up ~50% of the lipid chains in the retinal rod outer segment disk membranes and a large fraction of the lipid chains in the membranes of neuronal tissues. There is an extensive literature concerned with the dietary requirements for essential fatty acids and the importance of DHA to human health, but relatively little research has been done on the physical properties of this important molecule. Using ^{1}H and ^{13}C MAS NMR measurements of dispersions of 1-palmitoyl-2-docosahexaenoyl-phosphatidylcholine in excess phosphate buffer, we have unambiguously assigned most of the resonances in both the ^{1}H and ^{13}C NMR spectra. We were able to use cross-polarization spectroscopy to follow the transfer of polarization from specific ^{1}H nuclei not only to their directly bonded ^{13}C but also to those ^{13}C that are in close proximity, even though they are not directly bonded. Cross-peaks in two-dimensional cross-polarization spectra revealed a close association between the choline headgroup and at least part of the DHA chain but not with the palmitate chain. Finally, we examined the dynamics of the different parts of this lipid molecule, using rotating frame spin-lattice relaxation measurements, and found that methylene groups of both chains experience important motions with correlation times in the 10-μs range, with those for the palmitate chain being ~50% longer than those of the DHA chain. The choline headgroup and the chain terminal groups have significantly shorter correlation times, and that part of the dipolar interaction that is fluctuating at these correlation times is significantly smaller for these groups than it is for the palmitate and DHA chain methylenes.

INTRODUCTION

Extensive dietary studies have detailed the critical importance of the polyunsaturated fatty acid docosahexaenoic acid or DHA (C22:6n-3) to health (Birch et al., 1992; Salem, 1989). This fatty acid makes up ~50% of the lipid chains in the retinal rod outer segment disk membranes, and a similar fraction is found in neuronal tissue membranes (Stinson et al., 1991). There is an extensive literature concerned with the dietary requirements of essential fatty acids for the synthesis of DHA, but surprisingly little research has been done on the physical properties of this important molecule. More specifically, little is known about its precise function in the membrane or about the properties of DHA that make it indispensable (Mitchell et al., 1998).

There has been renewed interest in DHA in recent years, particularly with regard to its role in the function of rhodopsin in the rod outer segment disk membrane (Brown, 1994). Absorbance measurements have shown that the rhodopsin photointermediate MI-to-MII conversion equilibrium constant is dramatically reduced in dimyristoylphosphatidylcholine (DMPC) bilayers relative to its value in a mixed-chain phospholipid (1-palmitoyl,2-DHA-phosphatidylcholine or PDPC) bilayer (Litman and Mitchell, 1996). This has been interpreted as evidence for increased lateral compressibility and increased conformational freedom of the DHA chains relative to saturated chains, which more

readily permits the expansion of rhodopsin during this transition (Litman and Mitchell, 1996; Mitchell et al., 1998). A similar conclusion had been reached earlier as a result of flash photolysis experiments on rhodopsin in disk membranes compared to a series of different phosphatidylcholine reconstituted membranes (Brown, 1994; Wiedemann et al., 1988), where it was concluded that the polyunsaturated membranes adapt more readily to the configurational changes of rhodopsin at the MI-to-MII transition.

Molecular mechanics computer modeling studies of DHA have been interpreted as suggesting a more rigid and ordered character for the polyunsaturated DHA chain (Applegate and Glomset, 1986, 1991a,b). On the other hand, Rabinovitch and Ripatti (1991) argue that a polyunsaturated chain having double-bonded carbons separated by a single methylene group, the motif found in DHA, have "maximum flexibility" and are minimally sensitive to temperature. Both studies find a highly compact minimum energy state for the chain, however. By comparing x-ray and ^{2}H NMR measurements of lipid bilayer area compressibility, Koenig et al. (1997) were able to extract separately the compressibilities of the two acyl chains for DMPC, 1-steroyl,2-oleoyl-PC (SOPC) and 1-steroyl,2-DHA-PC (SDPC), and deduced that the DHA chain had the lowest compressibility modulus (i.e., it was the most easily compressed) of the chains studied. The conclusion reached was that membranes containing large concentrations of lipids having DHA chains would be able to adapt more readily to membrane protein structural changes such as that occurring in the rhodopsin MI-to-MII transition. Earlier ^{2}H NMR work by Baenziger et al. (1991) on a specifically deuterated diunsaturated phospholipid was interpreted as providing evidence for a rela-

tively rigid structure near the double bonds, whereas the work of Dratz and Holte (1992) on DHA was felt to suggest a more flexible chain structure. This view has been supported by more recent ^{2}H NMR work (Holte et al., 1995, 1996).

Another potential role for DHA is the promotion of domain formation in membranes containing significant concentrations of cholesterol (Mitchell and Litman, 1998; Huster et al., 1998). Fluorescence lifetime and differential polarization measurements revealed that the ordering effect, described in terms of the orientational distribution function of diphenylhexatriene (DPH), of 30 mol% cholesterol on DPH was dramatically reduced in bilayers containing di-DHA-PC compared to all other PC lipids (Mitchell and Litman, 1998). Comparing the shapes of these angular distribution functions for bilayers with or without 30 mol% cholesterol reveals that DHA chains reduce, and that di-DHA-PC almost completely eliminates, the influence of cholesterol on DPH ordering. This is interpreted in terms of a microdomain model where, for a mixture of di-DHA lipids and mixed-chain lipid (such as SDPC), the saturated chains associate with each other and with cholesterol in microdomains, leaving the domains containing the unsaturated chains largely unaffected by cholesterol. What happens with di-DHA-PC/cholesterol bilayers does not seem to be explained by the model, however. In view of the small effects observed, it is possible that the cholesterol is not well dispersed within the bilayers. NMR studies of the effect of cholesterol on the hydrocarbon chain order of phospholipid mixtures of PC, phosphatidylethanolamine (PE), and phosphatidylserine (PS) having either (18:0,18:1) or (18:0,22:6) chains have shown that 10 mol% cholesterol increases the order of all chains by 5–18%, depending on headgroup and chain unsaturation (Huster et al., 1998). The largest effect observed was for (18:0,18:1)PE, and the smallest was for (18:0,22:6)PS. At 25 mol% cholesterol they found that the increase in hydrocarbon chain ordering of the (18:0,22:6) chain lipids ranged from 25% for PC and 19% for PE to 15% for PS. These results suggest a preferential association of cholesterol with PC and a stronger effect of cholesterol for (18:0,18:1) lipids than for (18:0,22:6) lipids. The direct influence of cholesterol on the DHA chains cannot be deduced from these measurements, however, because the order parameters refer only to the 18:0 chains. Nonetheless, the presence of 10 or 25 mol% cholesterol still has a strong influence on lipid chain order in all cases, but there is clear evidence for preferential interaction with PC.

We present here a ^{1}H and ^{13}C NMR study of bilayers of 1-palmitoyl,2-DHA-PC (PDPC) in excess phosphate buffer. Ab initio calculations of the different conformations of 1,4-pentadiene, which is used to model the local configuration of DHA near the methylene groups, are presented. They show that the methylene group ^{13}C chemical shift is essentially the same for four of the six minimum energy configurations of the torsion angles, whereas the other two

have a significantly different chemical shift. The ^{13}C NMR spectrum then indicates that these two configurations very likely have low occupation probabilities. Using cross-polarization spectroscopy, we examine the chain configuration and find an association between parts of the DHA chain and the phospholipid headgroup that is not present for the palmitate chain. Finally, measurements of the spin-lattice relaxation rates of the different ^{1}H resonances show that the palmitate chains are richer in low-frequency motion than the DHA chains.

MATERIALS AND METHODS

Sample preparation

1-Palmitoyl-2-docosahexaenoyl-*sn*-glycero-3 phosphocholine (PDPC) was purchased from Sigma Chemical Co. (St. Louis, MO). The NMR samples were prepared by dissolving the dried lipid into a phosphate-H_2O buffer (pH 7) at a 4:3 lipid/buffer ratio. The samples were mixed in a glass vial, using a slender stainless steel stirring rod, and then transferred to a 7-mm zirconium rotor (Doty Science, Columbia, SC). The hydrated lipid sample was then centrifuged for less than a minute, and the rotor brim was wiped clean. Teflon tape was stretched along the long aurum end caps to ensure that they remained fixed when inserted into the rotor. The entire sample preparation was performed in a glove bag evacuated with N_2 gas to prevent oxidation of the DHA chains. Only during centrifugation was the sample exposed to air. The total weight of the sample used for the 1D and $T_{1\rho}$ experiments was 140 mg (80 mg of dry lipid), and the total weight of the sample used for the 2D experiments was 375 mg (215 mg of dry lipid).

Nuclear magnetic resonance methods

All NMR spectra were obtained with a home-built spectrometer operating at a [1]H Larmor frequency of 360 MHz (equivalent to a static magnetic field of 8.5 T). The magic angle spinning (MAS) probe was built using a 7-mm spinning assembly, stator plus housing, from Doty Science. The MAS rate was 2.2 kHz for all experiments described here. The ^{1}H and [13]C 90° pulse lengths were both nominally 5 μs, except that reduced power was used for the [1]H $T_{1\rho}$ experiments, so the [1]H 90° pulses were 9.0 μs. Experiments incorporating a Hahn echo used a reduced power with a length of 19.0 μs for the [13]C 180° pulse. When ^{1}H decoupling was used the r.f. field strength was 22.3 kHz. Generally, 2048 complex data points were acquired by using dwell times of 50 μs for ^{13}C and 100 μs for ^{1}H spectra. CYCLOPS phase cycling was used in all experiments. Spectra were processed using FELIX 97 (MSI, San Diego, CA).

The 1D cross-polarization (CP) spectroscopy sequence is initiated with a 400-ms-long low-powered pulse (with an amplitude of less than 1 kHz) to saturate a specific resonance in the proton dimension. A [1]H 90° pulse is then followed by a spin-locking pulse on the protons and a Hartmann-Hahn polarization transfer to the carbons (Fig. 1 *a*). Detection occurs in the carbon dimension in the presence of strong proton decoupling. In a one-dimensional saturation experiment, a single ^{1}H peak, for example, that associated with the double-bonded carbons on the DHA chain, is selectively saturated and then CP is performed. Saturating a select ^{1}H peak prevents it from enhancing the signal of local carbon nuclei, because it has no polarization to transfer. By taking the difference between saturation and normal CP experiments, one observes only the magnitude of polarization transfer from the saturated ^{1}H nucleus to the neighboring carbons. In the difference experiments, as the contact time is increased, the "volume of influence" of the selected proton increases. This not only increases the intensity of the existing ^{13}C peaks but also brings peaks from more distant ^{13}C nuclei into the spectrum. Measuring individual peak areas in the
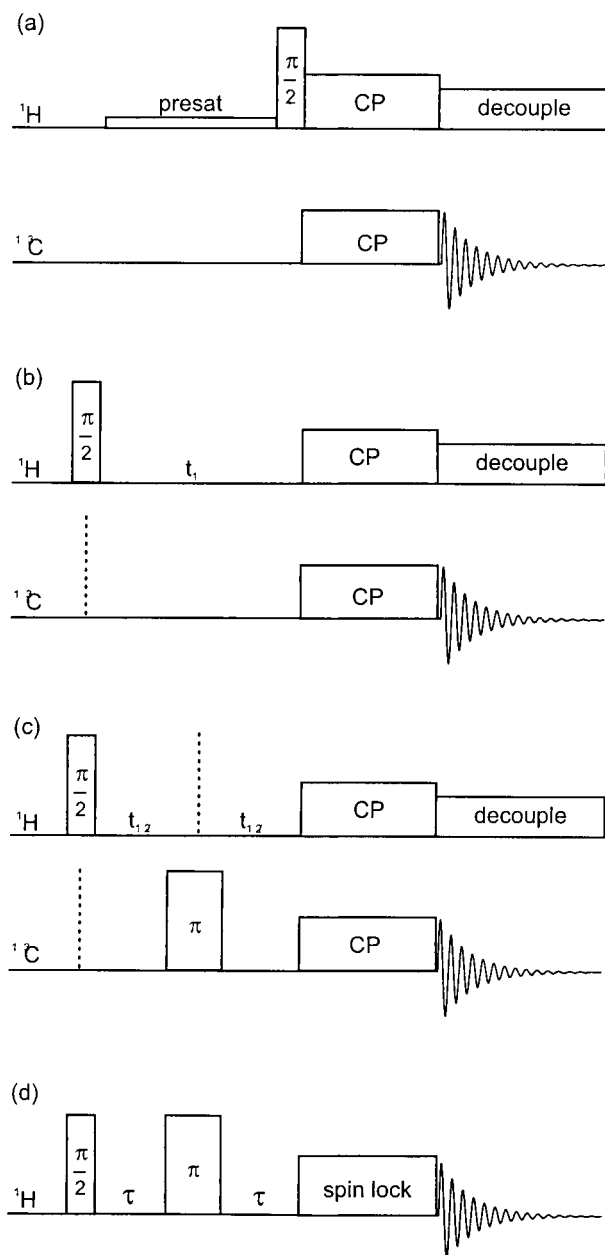
FIGURE 1   Some of the pulse sequences used in the various NMR experiments. (*a*) The 1D ^{1}H-^{13}C cross-polarization experiment with selective presaturation of specific ^{1}H resonances. (*b*) The basic 2D cross-polarization spectroscopy (CROPSY) experiment. The delay after the initial ^{1}H 90° pulse is the variable time t_1. (*c*) A variation of the CROPSY sequence shown in *b*. Here a ^{13}C 180° pulse is inserted during the middle of the variable interval t_1. (*d*) The sequence used to measure the ^{1}H relaxation rate in the rotating frame, $T_{1\rho}$. The first two pulses result in the formation of a Hahn echo, the signal of which is then spin-locked for a variable time τ.

difference spectra as a function of contact time allows the quantification of polarization transfer from the saturated proton to the carbon nuclei. The error in the peak area was determined by summing an area of the baseline equal to the width of a given peak and taking the standard deviation.

The proton saturation experiments were generalized to a 2D experiment in which spectra exhibited cross-peaks between the carbons and all of the protons that supplied polarization during CP. The 2D CP experiment, which is equivalent to the WISE (wide line separation) sequence of Schmidt-Rohr et al. (1992), consists of a ^{1}H 90° pulse followed by a variable delay t_1 before the CP pulses are applied (Fig. 1 *b*). Detection in t_2 is in the presence of strong ^{1}H decoupling. The protons directly bonded to the ^{13}C experience a J-coupling of ~140 Hz, which split the peaks in the proton dimension. All other nondirectly bonded protons that transfer polarization within the contact time give rise to a singlet cross-peak at the chemical shift of the donor proton and recipient carbon. To collapse the doublets due to heteronuclear ^{13}C-^{1}H J-coupling in the t_1 dimension, a 180° refocusing pulse is inserted into the middle of the t_1 interval (Fig. 1 *c*). All of the 2D CP spectra were obtained using a spectral width of 20 kHz in the direct (^{13}C) dimension and a t_1 increment of 0.2 ms (corresponding to a spectral width of 5 kHz) in the indirect (^{1}H) dimension. A total of 192 values of t_1 were collected in each experiment, and 132 scans, each having 2048 complex points, were acquired for each t_1. The recycle delay between scans was set at 3.5 s so that the complete experiment required in excess of 49 h. The States-Haberkorn-Ruben (1982) hypercomplex data sets were analyzed using Felix97. The direct dimension was zero-filled once to 4096 complex points, and the indirect dimension was zero filled to 1024 complex points. Sine-bell window functions were used in both dimensions for modest resolution enhancement. Proton and carbon resonances were assigned by tracking polarization transfer through the lipid at contact times of 1, 7, 15, 25, and 35 ms. To help determine which cross-peaks were due to the heteronuclear J-coupling between the ^{13}C and its directly bonded protons, a 2D spectrum was taken with a 180° ^{13}C refocusing pulse at the middle of t_1, using a contact time of 7 ms. The presence of this refocusing pulse resulted in the collapse of the doublets, aiding with the spectral assignment.

Because of the relatively slow spinning rate used for these experiments, 2.2 kHz, spinning side bands were observed in the ^{1}H NMR spectra and in the ^{1}H dimension of the 2D spectra. The spectrometer operating frequency was adjusted so that these were outside the spectral region of interest. Aliasing in the indirect dimension did not lead to any identifiable peaks in the region of interest. There were no observable spinning side bands in any of the ^{13}C 1D or 2D spectra.

The $T_{1\rho}$ pulse sequence begins with a ^{1}H 90° pulse followed by a 180° refocusing pulse. At the resulting Hahn echo maximum a variable-length spin-locking pulse is applied (Fig. 1 *d*). The ^{1}H magnetization is detected as a function of the length of the spin-locking pulse. $T_{1\rho}$ is proportional to spectral density at the effective field, ω_{eff}, determined by the strength of the applied r.f. field and the resonance offset frequency. We measured $T_{1\rho}$ for all accessible proton peaks in the spectrum at two separate effective fields. Peak area was measured using FELIX by summing the intensities of a proton peak as a function of spin-lock pulse time. $T_{1\rho}$ was determined using a three-parameter fit to a single exponential decay.

Ab Initio computations of chain conformations and chemical shifts

The ab initio calculations were performed using Gaussian98W (Frisch et al., 1998). For energy minimization and conformational mapping, energies were calculated with MP2, using the 6-31G** (6-31G(d,p)) basis set. For NMR chemical shift calculations the geometry was first optimized using the B3LYP density functional theory, and then the shielding tensors were calculated using the 6-31G** basis set (Foresman and Frisch, 1996; Cheesman et al., 1996).

RESULTS AND DISCUSSION

The overall chemical structure of PDPC and the labeling convention used to identify each of the atoms in the mole-

cule (Sudaralingam, 1972) are shown in Fig. 2. This drawing is not intended to represent the conformation of the molecule but is simply provided for reference to the chem-
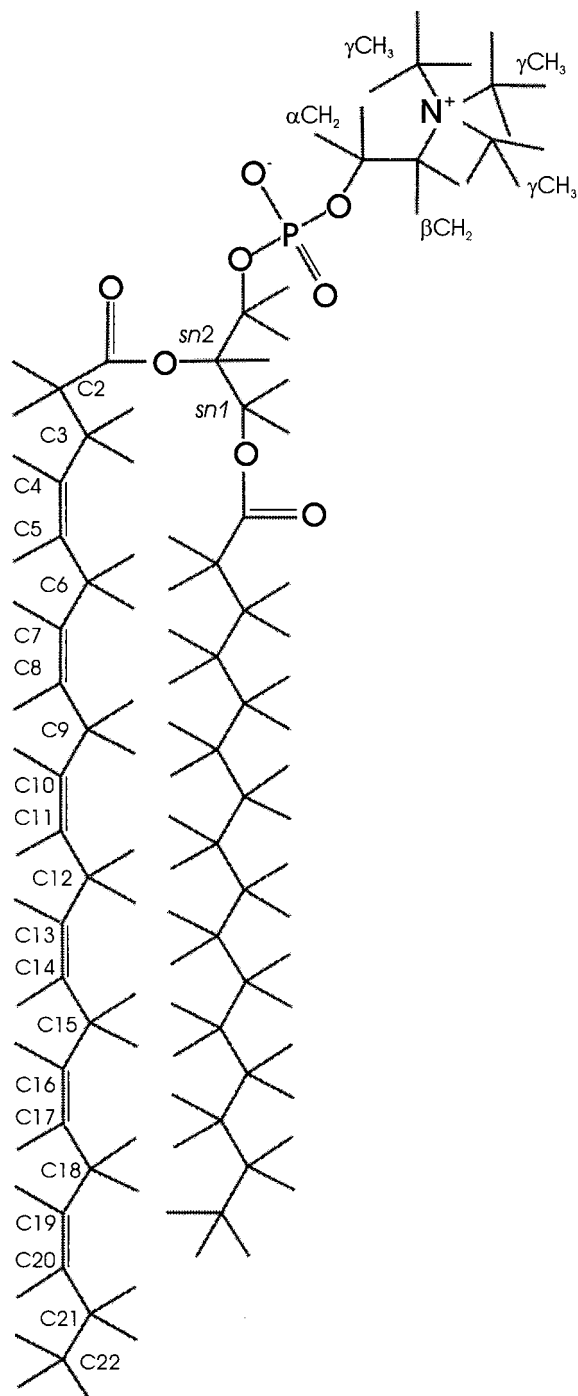

FIGURE 2 The chemical structure of 1-palmitoyl,2-docosahexaenoyl-*sn*-glycero-3-phosphocholine (PDPC). The nomenclature follows the convention of Sudaralingham (1972). This drawing is not intended to represent the conformation of the molecule, but simply to define the labeling of the atoms for the purposes of assigning the NMR spectra.

ical shift assignments for both ^{1}H and ^{13}C discussed later. The polyunsaturated DHA chain in particular is not expected to adopt the configuration shown. Displaying any other configuration for this chain would potentially mislead the reader, so we felt it best to display the molecule as shown. The atoms of the choline group attached to the phosphate (at the top of the figure) and those of the poly-unsaturated DHA chain will turn out to be the most interesting. In particular, we call attention to the pairs of olefinic carbons at positions (C4=C5), (C7=C8), (C10=C11), (C13=C14), (C16=C17), and (C19=C20) and to the methylene groups at positions C6, C9, C12, C15, and C18, which are "sandwiched" between the double-bonded carbon pairs. The methylene groups closest to the carbonyl groups connecting the chains to the glycerol backbone, the chain C2-CH$_2$ groups, will also turn out to be quite interesting. A molecule of this sort is expected to have a large degree of internal flexibility. In particular, at physiological temperatures within the fluid or liquid crystalline phase of natural membranes or model membrane systems, we expect to find a great deal of motion about all of the single carbon-carbon bonds. In comparison, rotation about the carbon-carbon double bonds is severely restricted.

The ^{1}H MAS NMR spectrum of a multilamellar dispersion of PDPC in phosphate buffer at pH 7, spinning at $\nu_R = 2.2$ kHz, at a temperature of 25°C, is shown in Fig. 3 *a*. The large resonance at ~4.7 ppm is due to the water. The ^{1}H spectrum is referenced to the headgroup's choline γ-(CH$_3$)$_3$ resonance, which is set at 3.26 ppm relative to tetramethyl silane (TMS). The resolution obtained with this sample is typical of multilamellar lipid/water dispersions under MAS conditions. With this resolution we are able to distinguish, for example, the two chain methyl groups, with chemical shifts of less than 1 ppm, and the two chain C2-CH$_2$ groups near 2.5 ppm. The resonance at 2.05 ppm is from the ^{1}H on C21 of the DHA chain, and that at 5.32 ppm is due to the ^{1}H on the double-bonded carbons, with a contribution from the ^{1}H at the glycerol C$_2$ position. The assignments of these peaks were made particularly easy by using the two-dimensional CP correlation experiment described below. Table 1 lists the assignments of both the ^{1}H and ^{13}C spectra.

The ^{1}H NMR spectrum in Fig. 3 *b* simply illustrates the effect of applying a long selective saturation pulse to the resonance at 5.32 ppm. The ability to saturate a particular resonance while leaving those nearby unaffected is central to the 1D CP difference experiments described later.

The ^{13}C MAS NMR spectrum shown in Fig. 4 was obtained from the same sample under the same experimental conditions as the ^{1}H spectrum of Fig. 3 *a*. The inset at the left of the figure is an expansion of the olefinic region of the spectrum. The ^{13}C NMR spectra are referenced by assigning the headgroup choline's γ-(CH$_3$)$_3$ resonance the chemical shift of 54.0 ppm relative to TMS. This spectrum was obtained using a simple Hahn echo (90°–τ–180°–τ–acquire) sequence, using cw ^{1}H decoupling (at an r.f. level of 22.3

TABLE 1 ^{1}H:^{13}C correlation matrix

δ^{1}H (ppm)		5.32	5.25	4.31	3.71	3.26	2.82	2.78	2.53	2.43	2.05	1.55	1.27	0.96	0.88
δ^{13}C (ppm)	Assign.	CH=CH	$CH=CH^*_{19}$	α-CH_2	β-CH_2	γ-$(CH_3)_3$	$(CC\text{-}CH_2\text{-}CC)_a$	$(CC\text{-}CH_2\text{-}CC)_b$	CH_2CO_a	CH_2CO_b	$C_{21}H_2$	$CH_2^*CH_2CO$	$(CH_2)_n$	DHA-CH_3	pal-CH_3
173.2	CO								s	s					
172.7	CO								s	s					
131.3	DHA-C_{20}										s				
128.4	C=C						s	s		s					
128.2	C=C						s	s		s					
128.0	C=C						s	s							
127.9	C=C						s	s							
127.7	C=C						s	s							
127.4	C=C						s	s							
126.8	DHA-C_{19}	s	d												
70.7	gly-C_2														
66.0	β-CH_2			s	d					s					
62.8	gly-C_1														
59.3	α-CH_2			d	s										
54.0	γ-$(CH_3)_3$					d	s								
33.8	pal-C^*H_2CO								d						
31.8	$C^*H_2CH_2CO$											d			
29.9	$(CH_2)_n$													s		
25.4	CC-C^*H_2-CC						d,s	d,s					s	s	
22.6	DHA-C^*H_2-CO									d			d		
22.5	pal-C^*H_2-CH_3												d	s	s
20.3	DHA-C_2,H_2										d			d	
14.0	DHA-CH_3													d	
13.8	pal-CH_3														d

s, cross-peak singlet; d, cross-peak doublet.

FIGURE 3 (*a*) A ^1H MAS NMR spectrum of PDPC. The sample spinning rate is $\nu_R = 2.3$ kHz, and 16 scans were averaged. The spectrum was referenced with respect to the $\gamma - (CH_3)_3$ resonance of the choline headgroup, which occurs at 3.26 ppm relative to TMS. (*b*) The same spectrum as in *a*, except that the resonance near 5.3 ppm has been saturated by a long, weak pulse applied at that frequency. This is the first stage in the measurement of 1D CP growth curves.
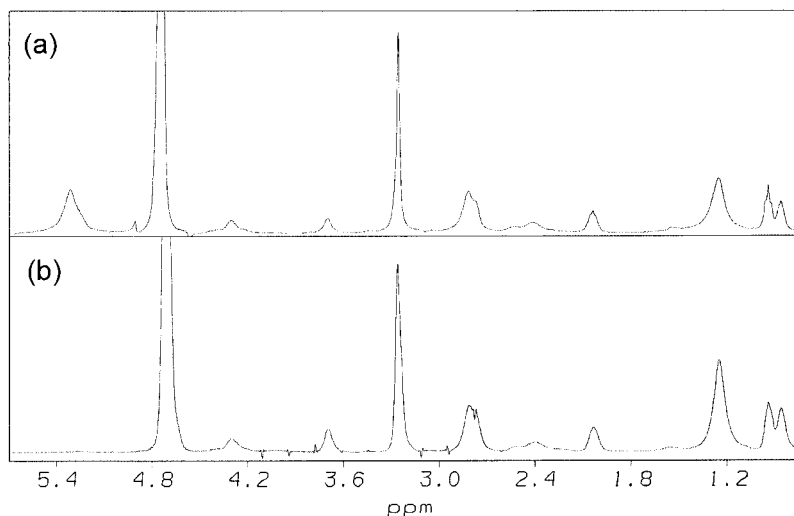
kHz) but no CP. One of the most obvious features of this spectrum is the resolution of at least seven of the 12 olefinic carbon resonances, which compares favorably with solution studies of polyunsaturated lipids (Aursand and Grasdalen, 1992; Sacchi et al., 1994). Another interesting feature, also seen in the solution spectra, is the very sharp resonance (having a linewidth of ~0.1 ppm, or 9 Hz) at 25.4 ppm. This single sharp line is due to the methylene group carbons C6, C9, C12, C15, and C18. In comparison, the $(CH_2)_n$ peak for the palmitoyl chain, found at 29.9 ppm, has a width of ~0.9 ppm.

The width of the palmitoyl methylene peak is due partly to the different population of *gauche* isomers at different chain positions. The precise chemical shift at any one position depends on the relative populations of the different conformers at that position; hence there is a distribution of chemical shifts. For a saturated fatty acid chain, the potential energy map as a function of torsion angle about the two

carbon-carbon bonds at a specific carbon position has three local minima at 180°, corresponding to the *trans* configuration, and ±60° corresponding to *gauche*$^+$ and *gauche*$^-$. The difference in chemical shift of the carbon atom at this position between the *trans* and *gauche* conformers of pentane, calculated using the ab initio program Gaussian, is ~2.1 ppm. Molecular dynamics simulations of liquid crystalline phase saturated chain lipids in a variety of environments (Belohorcova et al., 1999; Egberts et al., 1994; De Loof et al., 1991) give a distribution of *gauche* populations ranging from 0.12 to 0.30. This variation in the fraction of *gauche* isomers would result in a distribution of main-chain methylene carbon chemical shifts of ~0.4 ppm. The lack of any such distribution for the DHA chain suggests either that there is no variation in conformer population with chain position or that the chemical shifts corresponding to different conformers are very nearly the same. A similar ab initio calculation of the potential energy surface map for 1,4-

FIGURE 4 A ^{13}C MAS NMR spectrum of PDPC. The sample spinning rate is $\nu_R = 2.3$ kHz, and 2000 scans were averaged. No CP was used to acquire this spectrum. The ^{13}C magnetization was proton-decoupled, using continuous irradiation, with $\omega_1 = 22.3$ kHz, at the ^1H frequency during acquisition. The inset in the upper left-hand corner shows an expansion of the olefinic region of this spectrum.
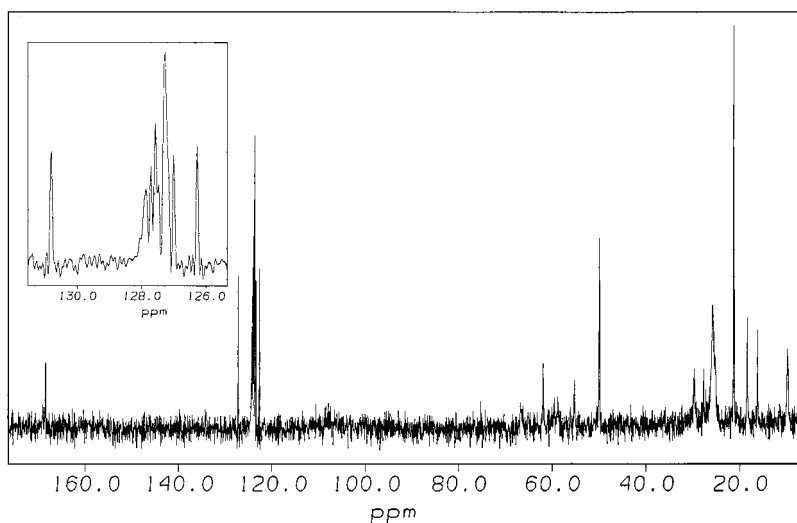
pentadiene, which has a single methylene group sandwiched between two pairs of double-bonded carbons, representing the motif found in DHA, shows local potential minima at $(\chi_1, \chi_2) = (117, 117), (-117, -117), (117, -117), (-117, 117), (115, -12),$ and $(-115, 12)$, in close agreement with the values reported by Applegate and Glomset (1986, 1991a,b) determined by molecular mechanics methods. The potential energy barriers between these minima are slightly smaller than the barriers between the saturated chain's *trans* and *gauche* conformers. The calculated chemical shift difference for the methylene carbon for the $(\pm117, \pm117)$ conformers of pentadiene is less than 0.2 ppm, while the conformers at $(\pm117, \mp12)$ have a chemical shift that differs by ~3.7 ppm. If the C6, C9, C12, C15, and C18 carbons of DHA sample primarily the $(\pm117, \pm117)$ conformations, we would not expect any significant variation in chemical shift among these carbons, even though the distribution of chain conformers may vary with chain position, as it does for saturated fatty acids.

Some of the other peaks in this ^{13}C spectrum, in particular those of the headgroup, will be discussed below when we describe the two-dimensional experiments. Table 1 provides a summary of all of the other peak assignments for both ^{13}C and ^1H.

Fig. 5 illustrates the one-dimensional polarization transfer difference experiment. The top trace (Fig. 5 a) is a normal CP ^{13}C spectrum taken in the absence of any ^1H presaturation pulse and shows the same features as the spectrum in Fig. 4. The remaining traces show difference spectra taken by subtracting the spectrum obtained using CP after first saturating the ^1H resonance at 5.3 ppm (the ^1H on the olefinic carbons) from the normal spectrum. The effect of the long saturation pulse on the ^1H spectrum is illustrated in Fig. 3 b, which, by comparison with the spectrum in Fig. 3 a, shows that the saturated resonance has disappeared, while the other resonances remain relatively unaffected.

Following this saturation pulse, the ^{13}C spins are cross-polarized for a contact time varying from 0.25 ms, for the trace second from the top, to 10 ms for the bottom trace. From such difference spectra we can see directly the contribution to CP from those ^1H spins that have been saturated.

The growth curves in Fig. 6 compare the growth in the intensity of the DHA chain methylene peak (at 25.4 ppm) as a function of contact time without presaturating any ^1H resonance (shown as *open circles*) in the presence of a presaturation pulse on the olefinic ^1H peak at 5.3 ppm (shown as *open squares*) and in the presence of a presaturation pulse on the DHA methylene ^1H peaks at 2.8 ppm (shown as *open triangles*). After a contact time of 8 ms, in the absence of presaturation the DHA methylene ^{13}C peak has reached 90% of its full intensity, compared to ~50% of its full intensity after that contact time when the olefinic ^1H peak was presaturated and ~35% of its full intensity when the DHA methylene ^1H peak was presaturated. Recall that the peaks observed in the "difference" experiment are from ^{13}C nuclei, which receive polarization only through their interaction with the "saturated" ^1H peak. This clearly demonstrates the importance of the nearby protons in the process of CP of the methylene ^{13}C nuclei. In principle it might be possible to quantitate this process by more systematic measurement of CP growth curves and to use this as a means of measuring the strength of the residual dipolar coupling between these nuclei, as has been done in solids (Muller et al., 1974; Mehring, 1983; Bizachew et al., 1994; Hirschinger and Herve, 1994; Tekely et al., 1995; Bertani et al., 1999).

Instead of selectively saturating individual ^1H resonances and collecting series of growth curves for individual ^{13}C peaks, it is possible to perform a two-dimensional version of this cross-polarization spectroscopy by inserting a variable delay between the initial ^1H 90° pulse and the start of Hartmann-Hahn CP, as illustrated in the pulse sequence of

FIGURE 5 A series of ^{13}C NMR difference spectra obtained using ^1H-^{13}C CP, after saturation of the olefinic ^1H resonances (CH=CH) near 5.3 ppm at different values of CP contact time. The top trace, *a*, shows the spectrum in the absence of any ^1H saturation, while the lower four traces show the difference between this spectrum and that obtained at different values of the CP contact time. Specifically, for the different traces the contact time was (*b*) 0.25 ms, (*c*) 1.5 ms, (*d*) 7.0 ms, and (*e*) 10 ms. A total of 1000 scans were accumulated for each of the above difference spectra.
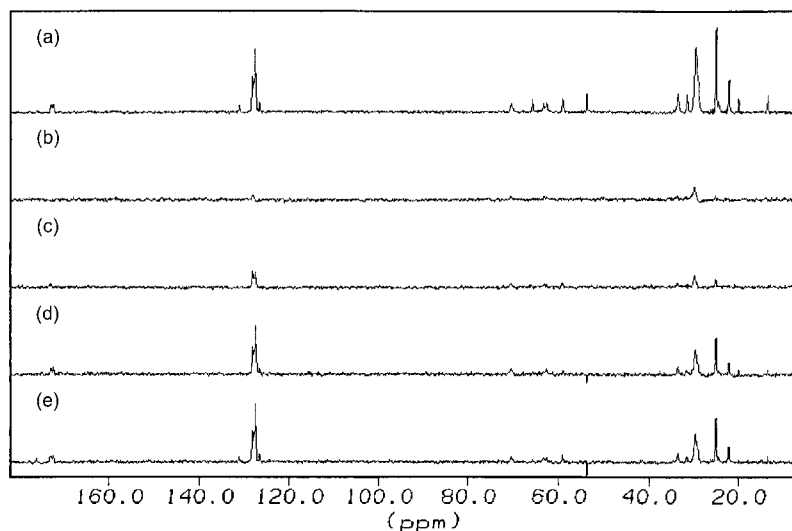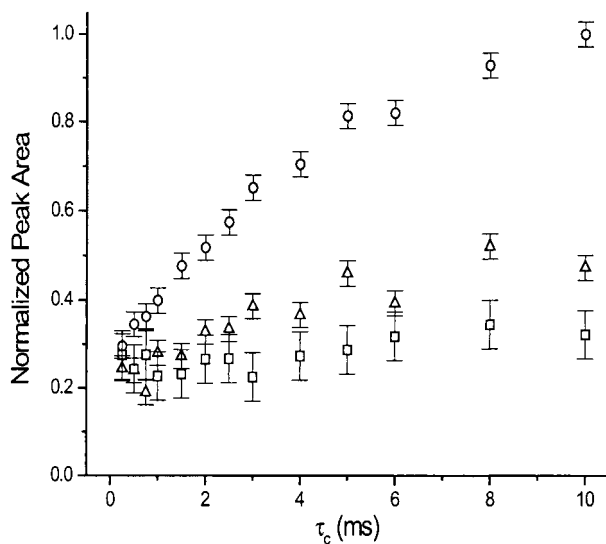
FIGURE 6   CP ^{13}C magnetization growth curves for the DHA chain methylene peaks (at 25.4 ppm), with no ^{1}H presaturation pulse (○) and after the olefinic ^{1}H resonances were saturated (□). Also shown is the growth curve for the olefinic carbon resonances (△) after saturation of the DHA methylene ^{1}H resonance near 2.8 ppm. Spectra were taken at 25°C.

Fig. 1 *b*. The ^{1}H precession during t_1 frequency encodes the ^{1}H magnetization, which is then transferred to the proximal ^{13}C nuclei by the Hartmann-Hahn contact (only the com-

ponent of magnetization that is parallel to the ^{1}H spin-locking pulse can cross-polarize the ^{13}C spins). A two-dimensional Fourier transform results in a ^{1}H-^{13}C correlation spectrum with peaks occurring for pairs of spins that are coupled either through their J-coupling or via their through-space dipolar coupling. An example of the 2D cross-polarization spectrum obtained in this fashion is shown in Fig. 7. Here we have plotted the region between 0.5 and 4.8 ppm in the ^{1}H dimension and between 10 and 75 ppm in the ^{13}C dimension. This region shows a number of the palmitic and DHA chain resonances as well as the phosphatidylcholine headgroup peaks.

Wherever there is a ^{13}C directly bonded to a ^{1}H nucleus, one sees a J-split doublet in the ^{1}H dimension. The center of the two peaks in these doublets gives the chemical shift of the ^{1}H to which the carbons are bonded. In the spectrum shown, which was taken with a contact time of 35 ms, there are also a number of singlet peaks corresponding to pairs of ^{1}H and ^{13}C spins that are not directly bonded but are interacting through space via the dipolar interaction. For example, the cross-peak at a ^{1}H chemical shift of 0.96 ppm and a ^{13}C chemical shift of 20.3 ppm is between the DHA chain methyl group protons and the DHA chain C21 carbon. Similarly, the singlet peak at a ^{1}H chemical shift of 4.3 ppm and a ^{13}C chemical shift of 66.0 ppm is between the head-group α-CH$_2$ protons and the neighboring β-CH$_2$ carbon.
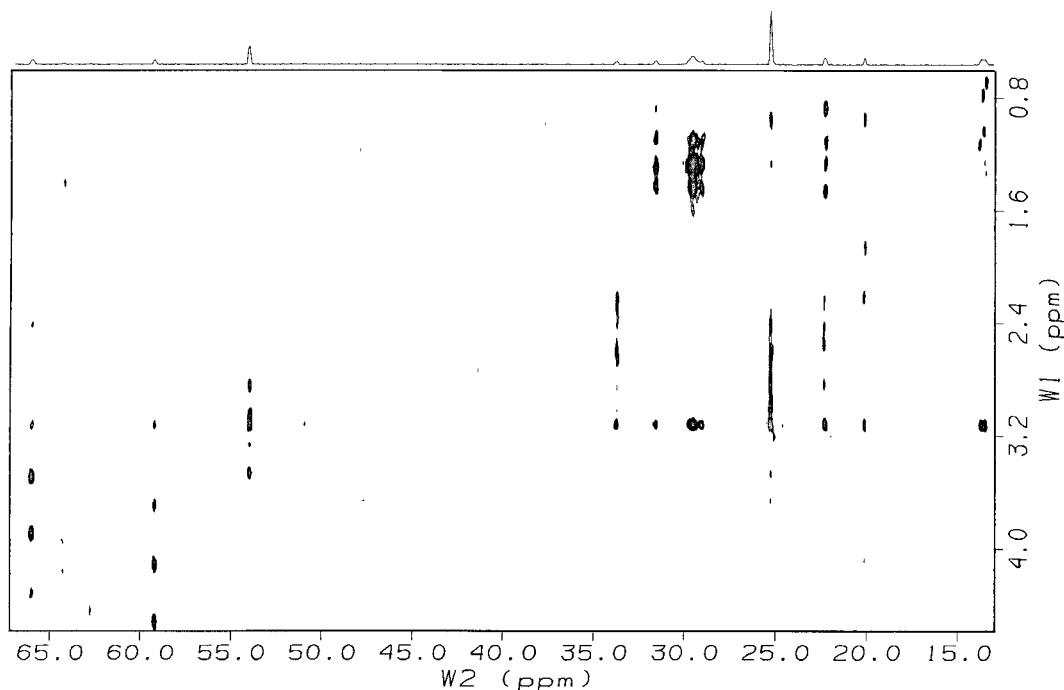

FIGURE 7   The region of the two-dimensional ^{1}H-^{13}C CROPSY correlation spectrum, taken with a mixing time of 35 ms, between 13 and 67 ppm in the ^{13}C dimension and 0.6 and 4.6 ppm in the proton dimension. This spectrum illustrates the effect of the heteronuclear J-coupling between the ^{13}C nuclei and their directly bonded ^{1}H. The projection shown at the top of the spectrum is the ^{13}C 1D spectra. Note that the J-coupling is visible in the ^{1}H dimension, only because of the decoupling during acquisition of the ^{13}C signal.
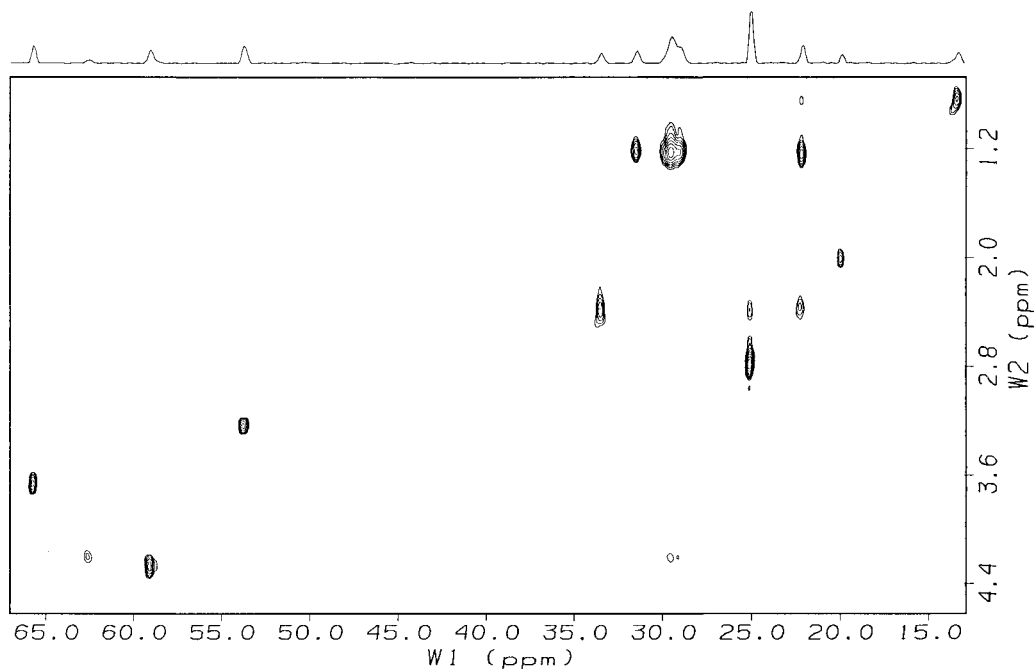
FIGURE 8 The same spectral region as that shown in Fig. 7, of a 2D CROPSY spectrum obtained using sequence c from Fig. 1, which has a [13]C 180° pulse inserted at the center of t_1 to refocus the heteronuclear J-coupling. The characteristic J-splittings in the ^{1}H dimension have been removed.

Other assignments of both the doublets and singlets in this spectrum are given in Table 1.

Fig. 8 shows the CP spectrum taken with the sequence in Fig. 1 c, which has a [13]C 180° pulse at the center of t_1. Recall that this pulse refocuses the precession due to the heteronuclear J-coupling during t_1, so that the spectrum does not show any splittings in the ^{1}H dimension. Comparison of these two spectra readily distinguishes the directly bonded [1]H-^{13}C spin pairs, facilitating the assignments. Careful examination of these spectra removes many ambiguities from the spectral assignments. For example, the cross-peak between the DHA C21 carbon at 20.27 ppm and the chain methyl group ^{1}H at 0.96 ppm identifies this as the DHA chain methyl group, and the doublet between this ^{1}H peak and the ^{13}C at 13.97 ppm in the unrefocused spectrum identifies it as the DHA chain methyl carbon. Similarly, the cross-peak between the palmitic chain [13]C15H_2 group carbon, at 22.45 ppm, and the chain methyl group ^{1}H at 0.88 ppm in the spectrum of Fig. 8 identifies it as the palmitic chain methyl, while the doublet between these ^{1}H and the carbon at 13.77 ppm in the spectrum of Fig. 7 identifies it as the palmitic chain methyl carbon.

Fig. 9 is an expansion of the region between 126 and 132 ppm in the ^{13}C dimension and 4.8 and 6.0 ppm in the ^{1}H dimension. This is the DHA chain olefinic region showing the resolution of seven of the 12 double-bonded carbons. The peak with the highest ^{13}C chemical shift belongs to C20, while that with the smallest chemical shift belongs to C19 (Sacchi et al., 1994; Aursand and Grasdalen, 1992).

The outer two peaks, in the ^{1}H dimension, of each of these carbons form the heteronuclear J-coupled doublet, while the inner peak is at the isotropic chemical shift position of the neighboring carbon's [1]H. Thus the arrows connect the inner
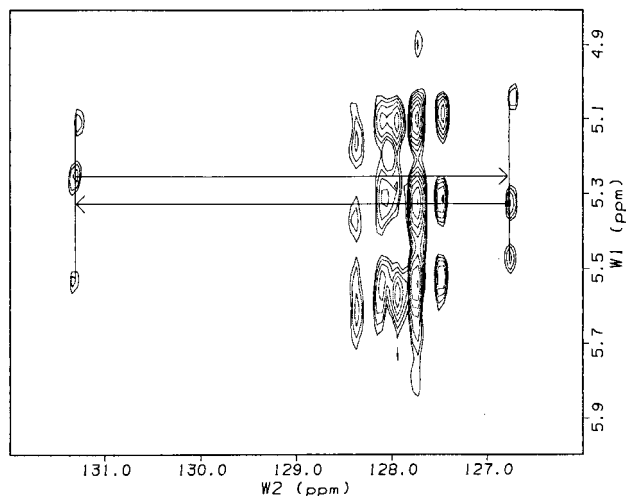

FIGURE 9 Expansion of the olefinic region of the two-dimensional [1]H-^{13}C CROPSY correlation spectrum taken with a mixing time of 7 ms. The doublets arise from the heteronuclear J-coupling between the ^{13}C nuclei and their directly bonded ^{1}H, while the singlets between the doublet peaks are due to through-space dipolar couplings. The arrows indicate the mutual dipolar coupling between ^{13}C nuclei at positions 19 and 20 of the DHA chain with the ^{1}H nuclei at the opposite positions (i.e., at positions 20 and 19, respectively).

peak for C20 to the center of the C19 doublet, and vice versa. Unfortunately, the resolution attainable does not allow us to carry the process further, so that we cannot assign all of the peaks in this region. The presence of a cross-peak between the C20 carbon at 131.34 ppm and the $C21^1H_2$ at 2.05 ppm confirms the previous assignment of these peaks.

Fig. 10 shows the polar headgroup region between 54 and 67 ppm in the ^{13}C dimension and between 2.1 and 4.9 ppm in the ^1H dimension. This spectrum, also taken with a contact time of 35 ms, shows the cross-peaks between neighboring α and β methylene groups on the choline headgroup. It also shows cross-peaks between the carbons of the γ-$(CH_3)_3$ group at 54.0 ppm and the DHA chain methylene group ^1H at 2.8 ppm. In addition, there is a cross-peak between the choline β-CH_2 carbon at 66 ppm and the DHA chain C2-CH_2 ^1H at 2.4 ppm. The presence of these cross-peaks between the headgroup and the DHA chain, and the absence of similar cross-peaks between the headgroup and the palmitic chain, suggest that at least part of the DHA chain is more exposed to the lipid-water interface region than the palmitic chain is.

The cross-peaks between the choline headgroup and the DHA chain indicate that at least part of the unsaturated chain is close to the lipid-water interface and the polar headgroup region. Longer contact times and an improved signal-to-noise ratio may eventually permit a more complete picture of the conformation of this molecule. The absence of
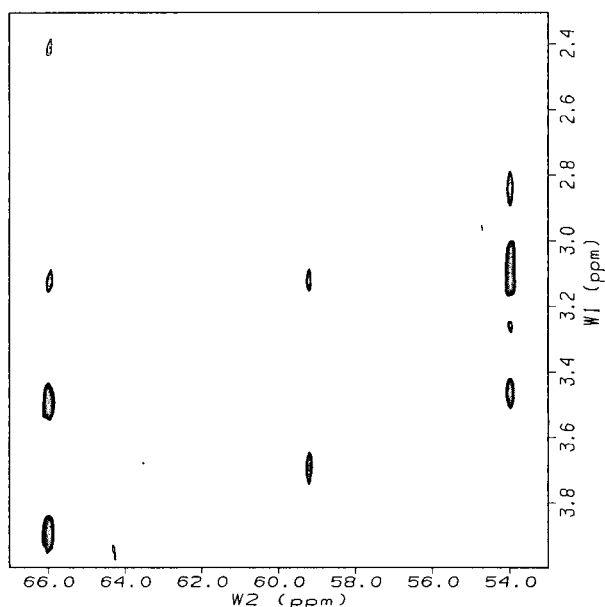
any significant variation with position of ^{13}C chemical shift for C6, C9, C12, C15, and C18 despite the relatively large theoretical difference in chemical shift, calculated by Gaussian, of the $(\pm 115, \mp 12)$ configurations compared to that of the $(\pm 117, \pm 117)$ configurations suggests that the former have a relatively low occupation probability. However, little can be said regarding the populations of or the rate of transition between the latter.

Some information about the lipid dynamics can be obtained from relaxation measurements, however. The rate of spin-lattice relaxation in the rotating frame, $1/T_{1\rho}$, is measured in the presence of r.f. irradiation of amplitude ω_1, at frequencies ω that are close to the Larmor frequency ω_0. The resonance offset frequency, $\Delta\omega = \omega_0 - \omega$, and the r.f. strength, ω_1, determine the effective precession frequency, and an effective field, in the rotating frame

$$\omega_{eff} = \sqrt{((\Delta\omega)^2 + \omega_1^2)} \tag{1}$$

We also define the parameter $\theta = \tan^{-1}(\omega_1/\Delta\omega)$. The rotating frame spin-lattice relaxation rate is most sensitive to fluctuations in the nuclear Hamiltonian that occur at frequencies near this effective field. The effective field is normally much smaller than the Larmor precession frequency, so that for systems that are rich in lower frequency motions (Stohrer et al., 1991; Davis, 1986) i.e., that have correlation times $\tau_c \gg 1/\omega_0$, the rotating frame relaxation time $T_{1\rho}$ is much shorter than the usual spin-lattice relaxation time T_1 (Qian, 1997; Le Guernevé and Auger, 1995). In this case, for random isotropic reorientation described by a simple exponential correlation function with a correlation time τ_c, we expect that the rotating frame spin-lattice relaxation rate for two like nuclei i and j, with nuclear gyromagnetic ratio γ, separated by a distance r_{ij} and interacting via their mutual dipolar coupling, will vary as (Abragam, 1961; Jones, 1966)

$$\frac{1}{T_{1\rho}} = \frac{9}{20} \frac{\gamma^4 \hbar^2}{r_{ij}^6} \sin^2\theta \left[\cos^2\theta \frac{\tau_c}{1 + \omega_{eff}^2 \tau_c^2} + \sin^2\theta \frac{\tau_c}{1 + 4\omega_{eff}^2 \tau_c^2} \right] \tag{2}$$

This result can be readily generalized for systems of more than two spins. For lipid bilayers and membranes, the molecular reorientations are not isotropic, so the expression for the rotating frame spin-lattice relaxation rate becomes more complex. In particular, it depends on the orientation of the bilayer normal relative to the magnetic field. For powder samples we measure a relaxation rate that is averaged over all orientations. In addition, that part of the dipolar interaction that is responsible for the rotating frame relaxation is the fraction, $\Delta M_2 = \overline{(\Delta\omega_0)^2}$, of the interaction that is modulated by orientational fluctuations with frequencies near ω_{eff} (Davis, 1995; Abragam, 1961). The bar indicates an average over motions in this frequency range. Unfortunately, we have no independent measure of this ΔM_2. For

FIGURE 10 The region of the two-dimensional ^1H-^{13}C CROPSY correlation spectrum, taken with a mixing time of 35 ms, in the choline headgroup region, from 53 to 67 ppm in the ^{13}C dimension and from 2.3 to 4.0 ppm in the ^1H dimension, showing the doublets due to heteronuclear J-coupling between the ^{13}C nuclei and their directly bonded ^1H, and the through-space dipolar coupling between the headgroup ^{13}C nuclei and the nearby, but not directly bonded, ^1H nuclei.

this reason we replace the expression in Eq. 2 with

$$\frac{1}{T_{1\rho}} = \mathcal{H} \sin^2\theta \left[\cos^2\theta \frac{\tau_c}{1 + \omega_{eff}^2 \tau_c^2} + \sin^2\theta \frac{\tau_c}{1 + 4\omega_{eff}^2 \tau_c^2} \right] \quad (3)$$

If we assume that the motion in this frequency range is reasonably well described in terms of a single average correlation time, τ_c, and a single value for the mean square fluctuation, $\mathcal{H} = \Delta M_2$, by measuring $T_{1\rho}$ at at least two different values of effective field, ω_{eff}, we can use Eq. 3 to determine both τ_c and $\mathcal{H}$.

It must be kept in mind, however, that for complex molecular systems with many internal and global degrees of freedom, such as phospholipid/water dispersions in the fluid phase, there are still important high-frequency motions and measurements of $T_{1\rho}$ (or of T_1) that cannot provide a complete dynamical description.

We have measured the values of the ^{1}H rotating frame spin-lattice relaxation times at two r.f. field strengths, $\omega_1 = 6.95 \pm 0.2$ kHz and $\omega_1 = 13.9 \pm 0.4$ kHz. The effective fields are calculated by including the resonance offsets for individual peaks as in Eq. 1. Fig. 11 shows some typical decay curves for two of these peaks at two different values of effective field. The open symbols refer to the DHA chain (-C=C-CH$_2^*$-C=C-)$_n$ resonance, at 2.8 ppm, and the filled symbols to the palmitic chain (CH$_2$)$_n$ resonance at 1.27 ppm. The curves in Fig. 11 *a* are at the lower effective field, $\omega_1 = 2\pi \times 6.95$ kHz, and those in Fig. 11 *b* are at the higher effective field, $\omega_1 = 2\pi \times 13.9$ kHz. The offset frequency for the 2.8 ppm resonance is $\Delta\omega = 2\pi \times 1.36$ kHz, while that for the 1.27 ppm resonance is $\Delta\omega = 2\pi \times 0.81$ kHz. The solid curves are three parameter fits to a single exponential decay for each case. The $T_{1\rho}$ measurements are summarized in Table 2, which gives the peak assignments, the $T_{1\rho}$ values, their uncertainties, and the deduced parameters τ_c and $\mathcal{H}$ for each peak. Fig. 12 illustrates the graphical method used to arrive at values and uncertainties for τ_c and $\mathcal{H}$ for the DHA chain (-C=C-CH$_2^*$-C=C-)$_n$ resonance. First, Eq. 3 is solved for $\mathcal{H}$, which is then plotted as a function of the parameter τ_c to yield the solid curves in the figure. These curves used the values of $T_{1\rho}$ obtained at the two effective fields. In this figure, the curve with its minimum at the lower value of τ_c is for the higher effective field, while that with the shallower minimum at higher τ_c is for the lower effective field. The intersection of these two curves gives the values of τ_c and $\mathcal{H}$ that are consistent with both experiments. The dashed curves give the range of values of $\mathcal{H}$ consistent with experimental error in $T_{1\rho}$ at the higher effective field, while the dotted curves give the range of values consistent with the uncertainty in $T_{1\rho}$ at the lower effective field. Thus the roughly trapezoidal region at the intersection of these curves gives the permissible ranges of τ_c and $\mathcal{H}$ consistent with the data. This analysis was performed for each of the peaks in Table 2.
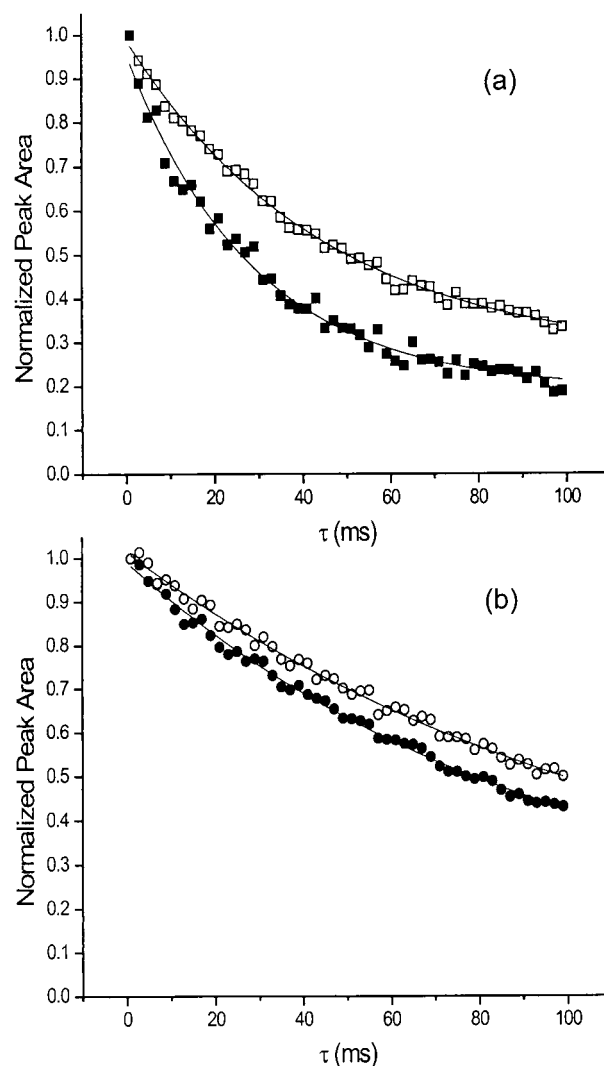

FIGURE 11 Examples of the ^{1}H $T_{1\rho}$ decay curves. (*a*) □, The decay of the magnetization of the DHA chain CH$_2$ groups (near 2.8 ppm); ■, the decay of the magnetization of the palmitic chain methylene CH$_2$ groups (near 1.27 ppm). These decay curves were taken with an applied spin-locking r.f. field of $\omega_1 = 6.95 \pm 0.2$ kHz. (*b*) □, The decay of the magnetization of the DHA chain CH$_2$ groups (near 2.8 ppm); ■, the decay of the magnetization of the palmitic chain methylene CH$_2$ groups (near 1.27 ppm). These decay curves were taken with a spin-locking field of $\omega_1 = 13.9 \pm 0.4$ kHz. The effective spin-locking field must also take account of the offset from resonance. Thus for *a* the effective spin-locking fields are actually $\omega_{eff} = 7.08 \pm 0.2$ kHz (□) and 7.0 ± 0.2 kHz (■), and for *b* they are 14.0 ± 0.2 kHz (○) and 13.9 ± 0.2 (●). The effects of the offset frequencies in this case are quite negligible.

The values of these parameters for the two DHA chain peaks are very similar, while the correlation time for the palmitic chain (CH$_2$)$_n$ peak and the value of $\mathcal{H}$ for that peak are ~50% larger. The larger value of $\mathcal{H}$ is undoubtedly due to the stronger interchain proton-proton dipolar interaction for the saturated chain. The longer τ_c implies a larger spectral density at longer time scales or more significant, slower motions on the palmitate chain. The shortest corre-

TABLE 2 Rotating frame relaxation ($\omega_1 = 2\pi \times 6.95$ kHz; $\omega_2 = 2\pi \times 13.9$ kHz)

Assignment	δ (ppm)	$T_{1\rho}[\omega_1]$ (ms)	$T_{1\rho}[\omega_2]$ (ms)	τ_c (μs)	$\mathcal{K}$ ($\times 10^6$ s^{-2})
Olefinic ^{1}H	5.32	118.3 ± 19.4	44.9 ± 1.1	12.7 ± 3.5	4.26 ± 0.1
Choline β-CH$_2$	3.71	90.1 ± 17.8	58.6 ± 2.8	8.9 ± 2.5	4.23 ± 0.4
Choline γ-(CH$_3$)$_3$	3.26	187.2 ± 15.8	72.0 ± 2.9	12.3 ± 1.8	2.53 ± 0.1
DHA-CC-CH$_2$-CC	2.78	116.4 ± 9.1	44.9 ± 1.1	12.25 ± 1.6	4.03 ± 0.1
DHA-C$_{21}$H$_2$	2.05	45.5 ± 0.1	28.9 ± 0.1	5.6 ± 0.3	7.91 ± 0.2
pal-(CH$_2$)$_n$	1.27	92.0 ± 5.1	28.8 ± 0.9	18.8 ± 1.3	6.87 ± 0.2
pal-CH$_3$	0.88	100.0 ± 15.5	48.8 ± 2.8	8.4 ± 2.0	3.78 ± 0.5

lation times are for the palmitate terminal methyl group, the DHA chain C21H$_2$ position (next to its terminal methyl group), and the choline β-CH$_2$ headgroup resonance. The small values of $\mathcal{K}$ for the choline γ-(CH$_3$)$_3$ group and the palmitate terminal methyl are a result of the very rapid methyl group motional averaging, which reduces the residual dipolar coupling at those positions. The absolute value of the parameter $\mathcal{K}$ amounts to only 1 or 2% of the residual dipolar second moment for a fluid phase phospholipid bilayer, which is $\sim 3.0 \times 10^8$ s^{-2} (MacKay, 1981). This residual fluid phase second moment is itself only a few percent of the rigid lattice proton dipolar second moment for lipid systems. It is clear that most of the motions responsible for the reduction of the rigid lattice second moment to its residual value in the fluid lipid phase are much faster than the correlation times listed in Table 2. Nonetheless, there are

important motions in this time scale range, and the difference between the two chains, DHA and palmitate, is significant.

CONCLUSION

Using ^{1}H and ^{13}C MAS NMR measurements of dispersions of 1-palmitoyl-2-docosahexaenoyl-PC in excess phosphate buffer, we have unambiguously assigned most of the resonances in both the ^{1}H and ^{13}C NMR spectra. We were able to use CP spectroscopy to follow the transfer of polarization from specific ^{1}H nuclei, not only to their directly bonded ^{13}C's, but also to those ^{13}C that are close to it in space. Cross-peaks in the two-dimensional CP spectra revealed that there was a close association between the choline headgroup and at least part of the DHA chain, but not with the palmitate chain. Finally, we examined the dynamics of the different parts of this lipid molecule, using rotating frame spin-lattice relaxation measurements, and found that methylene groups of both chains experience important motions with correlation times in the 10-μs range, with those for the palmitate chain being ~ 50% longer than those of the DHA chain. The choline headgroup and the chain-terminal groups have significantly shorter correlation times, and that part of the dipolar interaction that is fluctuating at these correlation times is significantly smaller for these groups than it is for the palmitate and DHA chain methylenes.

With improved sensitivity it should be possible to study more precisely the interaction between the ^{1}H and ^{13}C nuclei. Growth curves for many of the cross-peaks in the two-dimensional spectra could yield valuable information on the conformations and dynamics of the different parts of the molecule. Improved resolution would also permit identification of the rest of the resonances in the olefinic region of the ^{13}C spectrum and would help resolve the question of variation in chain dynamics with chain position for DHA. A more complete understanding of the structure and dynamics of phospholipids containing DHA chains may help to identify the key physical characteristics that make this such an important molecule for human health.
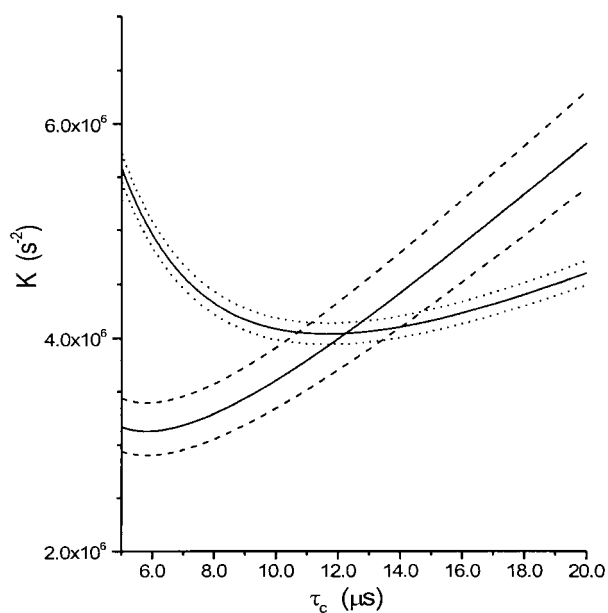

FIGURE 12 Determination of the correlation time, τ_c, and the mean squared amplitude of the fluctuation dipolar interaction, $\mathcal{K}$, responsible for the rotating frame relaxation rate. The solid curves are calculated from the values of $T_{1\rho}$ for the DHA chain methylene resonance at the two effective fields used. The dotted curves show the ranges corresponding to the respective experimental uncertainties in the values of $T_{1\rho}$. The curve with its minimum at the left side of the figure is for the data taken with $\omega_1 = 13.9$ kHz, and the curve with the shallower minimum is for $\omega_1 = 6.95$ kHz.

REFERENCES

Abragam, A. 1961. Principles of Nuclear Magnetism. Ch. VIII, Thermal relaxation in liquids and gases, pp. 264–353 and Ch. XII, The effects of strong radio-frequency fields, pp. 511–581. Oxford University Press, Oxford, U.K.

Applegate, K. R., and J. A. Glomset. 1986. Computer-based modeling of the conformation and packing properties of docosahexaenoic acid. *J. Lipid Res.* 27:658–680.

Applegate, K. R., and J. A. Glomset. 1991a. Effect of acyl chain unsaturation on the conformation of model diacylglycerols: a computer modeling study. *J. Lipid Res.* 32:635–644.

Applegate, K. R., and J. A. Glomset. 1991b. Effect of acyl chain unsaturation on the packing of model diacylglycerols in simulated monolayers. *J. Lipid Res.* 32:645–655.

Aursand, M., and H. Grasdalen. 1992. Interpretation of the ^{13}C-NMR spectra of omega-3 fatty acids and lipid extracted from the white muscle of Atlantic salmon (*Salmo salar*). *Chem. Phys. Lipids.* 62:239–251.

Baenziger, J. E., H. C. Jarrell, R. J. Hill, and I. C. P. Smith. 1991. Average structural and motional properties of a diunsaturated acyl chain in a lipid bilayer: effects of two *cis*-unsaturated double bonds. *Biochemistry.* 30:894–903.

Belohorcova, K., J. Qian, and J. H. Davis. 1999. Molecular dynamics and ^{2}H NMR study of the influence of an amphiphilic peptide on membrane order and dynamics. *Biophys. J.*, submitted.

Bertani, P., J. Raya, P. Reinheimer, R. Gougeon, L. Delmotte, and J. Hirschinger. 1999. ^{19}F/^{29}S distance determination in fluoride-containing octadecasil by Hartmann-Hahn cross-polarization under fast magic-angle spinning. *Solid State NMR.* 13:219–229.

Birch, E. E., D. G. Birch, D. R. Hoffman, and R. Uauy. 1992. Dietary essential fatty acid supply and visual acuity development. *Invest. Ophthamol. Vis. Sci.* 33:3242–3253.

Bizachew, D., L. C. M. Van Gorkom, I. G. Dance, J. V. Hanna, and M. A. Wilson. 1994. Cross-polarization dynamics in 2,6-dimethylbicyclo[3.3.1]nonane-*exo*-2-*exo*-6-diol inclusion compounds as studied by ^{13}C magic-angle spinning nuclear magnetic resonance spectroscopy. *Solid State NMR.* 3:67–78.

Brown, M. F. 1994. Modulation of rhodopsin function by properties of the membrane bilayer. *Chem. Phys. Lipids.* 73:159–180.

Cheesman, J. R., G. W. Trucks, T. A. Keith, and M. J. Frisch. 1996. A comparison of models for calculating nuclear magnetic resonance shielding tensors. *J. Chem. Phys.* 104:5497–5509.

Davis, J. H. 1986. The influence of membrane proteins on lipid dynamics. *Chem. Phys. Lipids.* 40:223–258.

Davis, J. H. 1995. High resolution ^{1}H nuclear magnetic resonance of a transmembrane peptide. *Biophys. J.* 69:1917–1932.

De Loof, H., S. C. Harvey, J. P. Segrest, and R. W. Pastor. 1991. Mean field stochastic boundary molecular dynamics simulation of a phospholipid in a membrane. *Biochemistry.* 30:2099–2113.

Dratz, E. A., and L. L. Holte. 1992. The "molecular spring" model for the function of 22:6ω-3 in biological membranes. *In* Essential Fatty Acids and Eicosanoids: Invited Papers from the Third International Congress. A. F. Sinclair and R. A. Gibson, editors. American Oil Chemists Society, Champaign, IL. 122–127.

Egberts, E., S. J. Marrink, and H. J. C. Berendsen. 1994. Molecular dynamics simulation of a phospholipid membrane. *Eur. Biophys. J.* 22:423–436.

Foresman, J. B., and A. Frisch. 1996. Exploring Chemistry with Electronic Structure Methods, 2nd Ed. Chap. 2, Single point energy calculations. Gaussian, Inc., Pittsburgh, PA. 13–37.

Frisch, M. J., G. W. Trucks, H. B. Schlegel, G. E. Scuseria, M. A. Robb, et al. 1998. Gaussian 98, Revision A.7. Gaussian, Inc., Pittsburgh, PA.

Hirschinger, J., and M. Herve. 1994. Cross-polarization dynamics and spin diffusion in some aromatic compounds. *Solid State NMR.* 3:121–135.

Holte, L. L., S. A. Peter, T. M. Sinnewell, and K. Gawrisch. 1995. ^{2}H nuclear magnetic resonance order parameter profiles suggest a change of molecular shape for phosphatidylcholines containing a polyunsaturated acyl chain. *Biophys. J.* 68:2396–2403.

Holte, L. L., F. Separovic, and K. Gawrisch. 1996. Nuclear magnetic resonance investigation of hydrocarbon chain packing in bilayers of polyunsaturated phospholipids. *Lipids.* 31:S199–S203.

Huster, D., K. Arnold, and K. Gawrisch. 1998. Influence of docosahexaenoic acid and cholesterol on lateral lipid organization in phospholipid mixtures. *Biochemistry.* 37:17299–17308.

Jones, G. P. 1966. Spin-lattice relaxation in the rotating frame: weak-collision case. *Phys. Rev.* 148:332–335.

Koenig, B. W., H. H. Strey, and K. Gawrisch. 1997. Membrane lateral compressibility determined by NMR and x-ray diffraction: effect of acyl chain polyunsaturation. *Biophys. J.* 73:1954–1966.

Le Guernevé, C., and M. Auger. 1995. New approach to study fast and slow motions in lipid bilayers: application to DMPC-cholesterol interactions. *Biophys. J.* 68:1952–1959.

Litman, B. J., and D. C. Mitchell. 1996. A role for phospholipid polyunsaturation in modulating protein function. *Lipids.* 31(Suppl.):S193–S197.

MacKay, A. 1981. A proton NMR moment study of the gel and liquid-crystalline phases of dipalmitoyl phosphatidylcholine. *Biophys. J.* 35:301–313.

Mehring, M. 1983. Principles of High Resolution NMR in Solids. Springer-Verlag, Berlin. 151–168.

Mitchell, D. C., K. Gawrisch, B. J. Litman, and N. Salem, Jr. 1998. Why is docosahexaenoic acid essential for nervous system function? *Mol. Struct. Phospholipids Regul. Cell Funct.* 26:365–370.

Mitchell, D. C., and B. J. Litman. 1998. Effect of cholesterol on molecular order and dynamics in highly polyunsaturated phospholipid bilayers. *Biophys. J.* 75:896–908.

Muller, L., A. Kumar, T. Baumann, and R. R. Ernst. 1974. Transient oscillations in NMR cross-polarization experiments in solids. *Phys. Rev. Lett.* 32:1402–1406.

Qian, J. 1997. The dynamics of peptide-16 in DMPC bilayer membranes: an NMR relaxation study. MSc thesis. University of Guelph, Guelph, Ontario.

Rabinovich, A. L., and P. O. Ripatti. 1991. On the conformational, physical properties and functions of polyunsaturated acyl chains. *Biophys. Biochim. Acta.* 1085:53–62.

Sacchi, R., I. Medina, L. Paolillo, and F. Addeo. 1994. High-resolution ^{13}C-NMR olefinic spectra of DHA and EPA acids, methyl esters and triacylglycerols. *Chem. Phys. Lipids.* 69:65073.

Salem, N., Jr. 1989. Omega-3 fatty acids: molecular and biochemical aspects. *In* New Protective Roles for Selected Nutrients. G. A. Spiller and J. Scala, editors. Alan R. Liss, New York. 109–228.

Schmidt-Rohr, K., J. Clauss, and H. W. Spiess. 1992. Correlation of structure, mobility and morphology by 2D WISE NMR. *Macromolecules.* 25:3273–3277.

Schmidt-Rohr, K., and H. W. Spiess. 1994. Multidimensional Solid-State NMR and Polymers. Academic Press, London. 213–216.

States, D. J., R. A. Haberkorn, and D. J. Ruben. 1982. A two-dimensional nuclear Overhauser experiment with pure absorption phase in four quadrants. *J. Magn. Reson.* 48:286–292.

Stinson, A. M., R. D. Wiegand, and R. E. Anderson. 1991. Fatty acid and molecular species compositions of phospholipids and diacylglycerols. *Exp. Eye Res.* 52:213–218.

Stohrer, J., G. Grobner, D. Reimer, K. Weisz, C. Mayer, and G. Kothe. 1991. Collective lipid motions in bilayer membranes studied by transverse deuteron spin relaxation. *J. Chem. Phys.* 95:672–678.

Sudaralingam, M. 1972. Molecular structures and conformations of the phospholipids and sphingomyelins. *Ann. N.Y. Acad. Sci.* 195:324–355.

Tekely, P., V. Gerardy, P. Palmes, D. Canet, and A. Retournard. 1995. Measurement of Hartmann–Hahn cross-polarization dynamics with quenching of T_{1P} relaxation dependence. *Solid State NMR.* 4:361–367.

Wiedemann, T. S., R. D. Pates, J. M. Beach, A. Salmon, and M. F. Brown. 1988. Lipid-protein interactions mediate the photochemical function of rhodopsin. *Biochemistry.* 29:6469–6474.